CROMSCI - Development of a Climbing Robot with Negative Pressure Adhesion for Inspections

C. Hillenbrand, D. Schmidt, K. Berns

January 31, 2008

Abstract

The non-destructive inspection of large concrete walls with autonomous systems is still an unsolved problem. One of the main difficulties is to develop a very flexible platform, which is able to move and inspect horizontal and vertical surfaces safely, fast and cost-efficient.

This report will present the climbing robot CROMSCI which is designed for the described task. The propulsion system consists of three omnidirectional driven wheels which are airproof and completely rotatable for a maximum of maneuverability. To detect critical situations each wheel is equipped with a load cell which can measure occuring forces and torques and allow force-balancing. The adhesion is done by a vacuum system of seven controllable vacuum chambers and one large reservoir chamber. Pressure sensors and valves are integrated for controlling which allows fast reaction on changing conditions. The rough and sharp-edged surface of concrete walls causes strong requirements concerning leak tightness and attrition to the sealing between vacuum chambers and walls. Therefore, each sealing must be flexible to allow a good adaption to the ground but also let the robot slip when it is moving.

1 Introduction

Regular inspections of concrete buildings like motorway bridges or dams are very extensive. E.g. the total number of these bridges in Germany is 32.300 with an average age of 33 years. To maintain the stability, safety of traffic and durability of these bridges regular inspections have to be performed every three, main inspections every six years. Among high expenses in money and time the technical staff has to work in hazardous environment by using complex access devices like free suspended enclosures or those mounted on telescopic cranes. For a better objectivity and reproducibility of inspections as well as for safe working conditions a climbing robot would be the best solution. With such a machine it is possible to check the building remote controlled or semi-autonomously.

In literature multiple kinds of climbing robots can be found using different adhesion and propulsion techniques. The easiest way to cling to vertical walls is via passive suction cups or magnetic adhesion [Fischer et al., 2007] [Brockmann, 2004]. These concepts do not fit because concrete walls are neither extremly smooth (like glass) nor ferromagnetic. Since several years researchers are building up gecko-like climbing robots which use vander-Waals molecular adhesion or kind of claws [Menon et al., 2004] [Autumn et al., 2005], but here the payload for different sensor systems as well as the velocity are too low. The

most confident technology for our application is the negative pressure adhesion. Climbing robots using this technology can be found in literature, although not all of them can be used for this application [Zhang et al., 2006] [Longo and Muscato, 2006] [Hägele, 2006] [Simons, 2006] [Luk et al., 2005]. Some of them are suitable only for flat surfaces or use legs for locomotion, which will result in slow movement. For climbing on concrete surfaces an active vacuum system driven by wheels seems to be the best solution because of fast continuous motion and a simple mechanical structure [Berns and Hillenbrand, 2001].

2 Configuration of CROMSCI

The major goal of this project is the development of a wheel driven service robot, which can cling to a wall via negative pressure [Hillenbrand and Berns, 2004]. It should be able to inspect the building area-wide and semi-autonomously under survey of a technician. For optimal movement the robot CROMSCI[1] is equipped with three single steerable and driven wheels as shown in figure 1. On an outer ring lies a movable manipulator arm which carries the sensors for inspection. The round shape with a complete diameter of $80cm$ is devided into seven single vacuum chambers for better adhesion attributes. Single losses of negative pressure can be balanced and the robot will not drop down. The overall weight is at about $25kg$, the maximum height is $40cm$.

2.1 Locomotion

As already mentioned CROMSCI uses an omnidirectional drive for locomotion. For our application a combination of three unsprung, driven and steerable wheels provides best characteristics for maneuverability and adhesion [Hillenbrand and Berns, 2006a]. The final prototype can be seen in figure 2. The complete inner cylinder is rotating driven by a normal DC Motor and equipped with the controlling circuit board. The electronic connection to the robot case is realized over a collector ring, strips are sealing the cylinder to the fixed case and keep the vacuum inside of the chamber.

The complete force which has to be applied by the wheels is about $386N$ resulting from weight ($\approx 250N$), seal friction ($\approx 88N$), driving resistance ($\approx 43N$) and vis inertiae ($\approx 5N$). Therefore modern torque motors are selected which produce $0.16Nm$ at $3500rpm$ and Harmonic Drives with a reduction of 121:1. This combination is able to generate continuously $182N$ per wheel by a maximum speed of $9.63m/min$ with $106mm$ diameter. Torque motors have the advantage that they can be overloaded for a short period, so that there are sufficient reserves for critical situations.

For indirect measuring forces at the wheel's contact point each wheel is equipped with an integrated load cell using strain gauges. They are designed to detect vertical forces (z-direction) up to $\pm 1.500N$ and transverse torques (x/y-direction) up to $\pm 150N$ with a high accuracy ($\pm 2\%$). The load cell is positioned $120mm$ above the driven wheel - all existing forces are going through the cell - so the robot is able to recognize whether downforces are too high for movement or dangerously low.

For localization our robot uses three different sensor systems: The easiest way is to calculate the robot's pose out of the detected wheel turning (wheel encoders). This may cause problems if the wheels are temporarily in an illegal state which will cause undetectable sideward slip of the wheels. Additionally an inertial measurement system which

[1] CROMSCI: Climbing RObot with Multiple Sucking Chambers for Inspection tasks

detects accelerations [Koch et al., 2005] and an active landmark sending laser impulses [Hach, 2006] are realized.

2.2 Configuration of the negative pressure system

The adhesion system of our climbing robot CROMSCI consists of seven single vacuum chambers which are supported by one large reservoir chamber at the top of the robot (figure 3). The number of working chambers is a good compromise between realization simplicity (best: only one chamber) and operation safety (best: as much chambers as possible). Each chamber with a volume of about $4.5l$ receives its negative pressure from the reservoir ($\approx 20l$) which is evacuated by three strong suction engines. The air-pressure in each chamber and the reservoir is measured by sensors. These informations are given to a close-loop controller which opens and closes valves to evacuate the chambers separately depending on the actual leak tightness. The total effective suction area of CROMSCI is $0.4m^2$, the pressure difference of the chambers is between $-50mbar$ and $-100mbar$ compared to ambient pressure. If one or more working chambers are loosing negative pressure they can be isolated from the vacuum system by closing the valve to avoid the propagation of normal pressure to the other chambers which will result in loss of adhesion.

Beside the real adhesion mechanism a thermodynamical model (section 3.1) has been created both to set up a close-loop controller and to simulate the airflow and pressure variations with modelled leakage areas.

An important aspect is the interaction between adhesion system and drive due to the fact that the robot should neither stuck to the wall (soft sealings) nor fall down (hard and robust sealings). So we have to make a compromise and allow controlled leakage to get good sliding characteristics and to develop special sealings which are wear-resistant, leak-proof and easy sliding. It is an assembly of a Butyl seal-bearer and two clamping profiles. It is possible to vary the height of the bearer by changing the air pressure inside. Onto the surface of the bearer different samples of seal material can be applied to find the optimum in friction and wear. The lift/drag ration and the value of friction have been tested on a Pin-on-Disc test stand [Hillenbrand et al., 2007].

2.3 Inspection System

For the inspection of the surface different sensors can be used. The cover meter is the most common method to detect rebars in the concrete. Another sensor is an impulse radar which detects holes inside the concrete which were made for wires inside of prestressed concrete bridges. Finally a high-resolution camera is used to detect cracks of $0.2mm$ width. An overview of sensor technologies which can be used to inspect concrete walls and which are adaptable to a mobile robot is introduced in [Weise et al., 2001].

To carry and utilize the inspection sensors they must be attached to a movable manipulator [Hillenbrand and Berns, 2006b]. The most compact and best solution for our robotic system is to use round guides with two driven sledges and to realise the motions in the x-y-plane with a parallel kinematic. Therefore, one arm is mounted on each sledge with passive bearings and both arms are merged together at the head (figure 1) to allow motions in all three directions and a rotation of the head. This solution has the advantage, that the middle of the robot is still usable for other robot components like the vacuum chambers. The disadvantages are the non-rectangular working space which leads to a more extensive motion control software and correlations between motion elements which

have to be balanced out.

3 Adhesion System

Beside the configuration of the negative pressure system, it must be modelled physically to understand how the robot can climb on concrete surfaces. Based on this theory a control architecture will be developed, which is able to detect leakages and prevent from losing adhesion.

3.1 Fundamentals

The chambers are sliding over the surface and are sealed with a flexible packing. Physically a chamber is open to the concrete surface, whereas the rest of the space is covered by hard plates. If the chamber will be evacuated a certain pressure difference $\Delta p = p_i - p_o$ between inside and outside of the chamber occurs (figure 4). Forces to all areas $F = \Delta p \cdot A$ will be generated, which can be summarized to a central force $\vec{F}_{cx\_z}$ comparable to a generated force by the effective area A_e. The resulting force can be adjusted via the pressure and takes effect in the fixed center of gravity of each effective area. If all seven chambers are working together its intensity and point of effect can be tuned. This mechanism allows the control system to optimize the pressure force to obtain good wheel balance for the drive system.

The first fundamental theorem of thermodynamics can be used to model the air flow. If it is simplified, equation (1) describes the change of pressure $\dot{p}_0$ inside to outside of each chamber, depending on the volume V, the temperature T, adiabatic exponent κ, gas constant R and the different mass flows $\dot{m}_k$ over chamber limits. The mass flow can take place over controlled valves or leakages between the seal and the wall.

$$\dot{p}_0 = \frac{\kappa \cdot R \cdot T}{V} \sum_{k=1}^{N} \dot{m}_k \tag{1}$$

The air flow between two volumes can be modelled by an airtube (figure 5). With Bernoulli's equation and neglect of gravity the flow of a medium with density ρ between two control areas A_{in} and A_{out} is

$$\frac{1}{2}\left(c_{out}^2 - c_{in}^2\right) + \int_{p_{in}}^{p_{out}} \frac{1}{\rho} dp + \int_0^1 \frac{\partial c\,(t,s)}{\partial t} ds = 0 \tag{2}$$

where air pressures p_{in}, p_{out} and air velocity c_{in} are known and c_{out} has to be found. By assuming a stationary flow (no change of velocity along s) the inertial term $\int_0^1 \frac{\partial c(t,s)}{\partial t} ds$ can be neglected. Furthermore it can be shown that the error by assuming $\rho = const$ is about 6% for the relevant pressure differences between A_{in} and A_{out}. Finally it is obvious that in each control volume a place exists where the air flow is zero. So it can also be assumed $c_{in} = 0$, which leads to

$$c_{out} = \operatorname{sgn}(p_{in} - p_{out}) \cdot \sqrt{2\frac{|p_{in} - p_{out}|}{\rho}} \tag{3}$$

where the sign of the difference (*sgn*-function) gives the direction of air flow and the argument of the square root only considers the absolute value $\Delta p = |p_{in} - p_{out}|$.

Considering the volume, the mass flow $\dot{m}_k = \rho \cdot c_{k\perp} \cdot A_k$ with velocity c_k perpendicular to control area A with density ρ can be converted with the result of equation 3 to obtain following formula - assuming $c_k = c_{k\perp}$:

$$\dot{m}_{k\_incompressible} = \mathrm{sgn}(p_k - p_0) \cdot A_k \sqrt{2 \cdot \rho \cdot |p_k - p_0|} \tag{4}$$

Equation 4 describes the mass flow through a control area A_k driven by a pressure difference $\Delta p = |p_k - p_0|$ of air between the volumes on the two sides of A_k.
With equation 1 this result leads to

$$\dot{p}_0 = \frac{\kappa \cdot R \cdot T}{V} \sum_{k=1}^{N} \left(\mathrm{sgn}(p_k - p_0) \cdot A_k \sqrt{2 \cdot \rho \cdot |p_k - p_0|} \right) \tag{5}$$

which describes the pressure change in one vacuum chamber as result of all coming and going mass flows. For the seven working chambers mass flows are caused by leakages of the sealing with a flow-effective leakage area $A_{l\_x,y}$ between chamber x and neighbor y and by opening the valve to the reservoir chamber with a flow-effective area A_{v_x}. According to equation 5 and figure 3 the differential equation for the pressure change in chamber 1 is:

$$\begin{aligned} \dot{p}_1 = \tfrac{\kappa \cdot R \cdot T}{V_1} \cdot \sqrt{2\rho} \cdot \quad & \Big[\mathrm{sgn}(p_O - p_1) \cdot A_{l\_1,0} \cdot \sqrt{|p_0 - p_1|} \\ & + \mathrm{sgn}(p_2 - p_1) \cdot A_{l\_1,2} \cdot \sqrt{|p_2 - p_1|} \\ & + \mathrm{sgn}(p_7 - p_1) \cdot A_{l\_1,7} \cdot \sqrt{|p_7 - p_1|} \\ & + \mathrm{sgn}(p_6 - p_1) \cdot A_{l\_1,6} \cdot \sqrt{|p_6 - p_1|} \\ & - \mathrm{sgn}(p_1 - p_R) \cdot A_{v\_1} \cdot \sqrt{|p_1 - p_R|} \Big] . \end{aligned} \tag{6}$$

where V_1 is the chamber volume and p_i is the chamber pressure according to the mentioned numbering scheme, A_{v_1} is the opening area of valve 1, p_R is the reservoir pressure and p_0 the ambient air pressure. The differential equations for chambers 2 to 6 are the same except for the indices. For the reservoir chamber mass flows come from open valves to the working chambers, an open exterior valve (which connects the reservoir to the environment) and from the exhaust by the suction engine. Therefore the differential equation for the reservoir pressure change is

$$\begin{aligned} \dot{p}_R = \tfrac{\kappa \cdot R \cdot T}{V_R} \cdot \quad & \Big\{ \sqrt{2\rho} \cdot \Big[\mathrm{sgn}(p_0 - p_R) \cdot A_{v\_R} \cdot \sqrt{|p_0 - p_R|} \\ & + \sum_{i=1}^{7} \left(\mathrm{sgn}(p_i - p_R) \cdot A_{v\_i} \cdot \sqrt{|p_i - p_R|} \right) \Big] - \rho \cdot \dot{V}_g \Big\} . \end{aligned} \tag{7}$$

where A_{v_R} is the opening area of the exterior valve and $\dot{V}_g$ is the volume flow taken away by the suction engine.

The chamber pressures p_i are measured by sensors which are calibrated to detect air pressure differences within a range of $-350mbar$ to $0mbar$ what is sufficient for this application. The overall error lies within $\pm 2mbar$ and can be neglected. For regulating the chamber pressure special valves are used which utilize regular stepper motors for opening and closing. The total area of each valve is $300mm^2$ and it can be opened or closed within $0.5s$.

3.2 Negative Pressure Control

Figure 6 shows the structure of the implemented close-loop control system which consists of several control levels [Wettach et al., 2005]. The *pressure force determination* is the highest module. It gets the overall forces and torque moments that affect the robot and its velocity. From these inputs the module calculates the necessary value and working point of the total pressure force to compensate these forces and torques in order to keep the robot balanced on the surface.

For the validation of the simulation system, a simple force model is used. Naturally this model has to be refined with regard to different environmental conditions, but this task is decoupled from the assessment of the adhesion system. On the next level the *leakage estimation* module calculates the leakage area of each working chamber based on the actual chamber pressures and valve areas. For chambers 1, ..., 6 the calculation uses equation 6 in which only leakage areas between chamber and environment are estimated. Based on this the *determination of active chambers* module computes which chambers cannot be evacuated any more due to a big leakage area. Finally the *total pressure force calculation* module determines from the actual chamber pressures the actual total pressure force that affects the robot. From all these inputs the *reference pressure determination* module calculates the reference pressures for each working chamber. Non-active chambers get the outside pressure as target. On the bottom level there is a common control loop for each working and the reservoir chamber where a *PID controller* calculates the reference valve areas based on the difference between desired and actual chamber pressures. Naturally the controller parameters for the reservoir chamber differ from those of the working chamber because of its greater volume and the effect that the reservoir pressure increases when the reservoir valve is opened.

The *valve actuator* module translates each valve area in a reference valve position as input for the *plant simulation*. Here the *valve simulation* module computes the new valve position and corresponding valve area based on the reference input and the elapsed time. With the actual valve areas the *vacuum system simulation* module calculates the new chamber pressures according to equation 6 and 7 which are the outputs of the plant simulation. Of course, in reality the chamber pressures come from pressure sensors.

3.3 Control Architecture

The pressure control is embedded into an overall control architecture of Cromsci which consists of different processing units organized in hierarchical layers as shown in figure 7. The top-layer is the workstation, which offers a graphical user interface and a special input device and interacts via ethernet with the onboard PC. This embedded PC is responsible for kinematic calculations, force control, trajectory movement and robot's security - organized in different software layers. Some sensors like a webcam or a laserscanner are connected directly to the embedded PC via USB, Firewire or Serial Port, whereas the load cells, encoders and motors are connected via CanBus and circuit boards.

The used circuit board consists of a digital signal processor (DSP) Freescale 56F803 which is cooperating with a complex programmable logic device (Altera EPM70256). Additionally there are supply parts, CanBus elements and amplifiers for the motors. The DSP is able to preprocess different types of sensors and to control up to two DC motors. Several DSP units are connected via CanBus to the embedded PC which is placed inside the robot case. Interface boards are used to communicate by means of serial peripheral interface (SPI) or general purpose IOs. We are using different board-periphery

combinations, e.g. manipulator control (DC motors, encoders), omnidirectional drive (DC motors, encoders, load cell) and negative pressure system (pressure sensors, valves).

In order to perceivc informations about the environment different sensor systems will be applied as shown in figure 7: Infrared sensors for detection of deep cracks or an abyss, ultrasonic sensors for obstacle detection, a Hokuyo laserscanner to detect salient structures which can not be negotiated by the robot, a cover meter for inspection, an inertial measurement system for localization, a light-section camera to get informations about the roughness of the surface and a webcam for user vision.

The software structure bases on the Modular Controller Architecture (MCA), which is a modular, network transparent and real-time capable C/C++ framework for controlling robots [Scholl et al., 2001]. The control software provides different motion and inspection behaviors which can be activated by the user. These behaviors abstract from real robot hardware and are combined with some basic security behaviors which can slow the robot down or turn it away if the current state could lead to a critical situation. An abstraction layer transfers values from the abstract behavioral into the robot's space by concerning its internal parameters. Here is the kinematic calculation done as well as sensor preprocessing and force control.

4 Experiments

The functionality of the introduced principles has been presented before by using one-chamber prototype both in simulation and in real experiments. The presented seven chambers are currently working only inside the simulation. Therefore the shown experiments concerning close-loop control of negative pressure are done in our simulation environment. The air flow is simulated by the introduced thermodynamic modell. The visualization is done via the framework SimVis3D [Braun et al., 2007] and can be seen in figure 8. Real-life experiments with the seven-chamber prototype are still missing because the mechanical construction of Cromsci has not yet been completed.

4.1 Test Results of One-Chamber Prototype

Experiments with the one-chamber prototype are shown in figure 9. This prototype only consists of a single working chamber with a diameter of $30cm$ and one reservoir chamber. Each chamber is equipped with a pressure sensor and a valve as described above, an external suction engine is used to generate the negative pressure [Schmitz, 2005].

For the experiments a wooden plate with holes of different diameters is used and the progress of valve area and chamber pressures is logged. The upper image shows the system's behavior while driving across a $4mm$ hole (leakage $\approx 12mm^2$). At first the working chamber is inactive (closed valve) and the robot is held manually. After this the valve is opened and the working chamber becomes evacuated. From time $t = 6$ the control system balances the pressure by opening and closing the valve, after this the robot passes an edge between two plates and the valve is opened to maximum. After a short time of normal controlling the robot arrives at the hole ($t = 15$) and the working chamber's valve is opened to maximum again - but the negative pressure is still strong enough for safe adhesion.

Experiments with larger leakages result in much higher pressure values than before so the downforce is lower. As a result the wheels slip and the robot stucks at the current position but fortunately does not fall down.

4.2 Simulation Environment

For simulating the behavior of the negative pressure system the airflow between a vacuum chamber and the environment caused by leakages must be determined. Because of the robot's application leakages arise because of grooves, holes, pores connected through capillary channels, cracks, steps between two concrete slabs and protrusions caused by out-pouring of concrete between paling-boards.

In the simulation model all these phenomena are summarized as a crack of a certain width and depth. Furthermore, the roughness of concrete and sealing surface can be approximated by modelling a crack along the chamber edge of depth $0.1mm$ called basic leakage. The leakage area caused by an arbitrary crack depends on the geometry of the crack and the base area of the chamber which has contact with that crack. Based on this all leakage areas $A_{k_{in}}$ can be calculated and equation 5 can be used to simulate pressure alteration.

Basis of the pressure simulation is the model of a circular climbing robot with the already described chambers and valves. According to equation 5 the relevant mass flow for each chamber either comes from an open valve or from a leakage area caused by a crack. As the pressure difference between two volumes connected by a leakage has to be calculated, the leakage area of each chamber has to be determined separately for each counterpart volume (neighbor chamber or environment). Figure 3 shows the model for the chamber system of the robot with numbered chambers (1..7). Furthermore, an exemplary crack is shown which intersects chambers 1 and 7: in this situation leakage areas have to be calculated for edges $E_{0,1}$ and $E_{1,7}$. In this situation the leakage model has an important consequence: only chamber 1 is connected to the environment but not chamber 7. So in each case chamber 7 can only get in contact with the six surrounding chambers but not directly with the environment. Therefore, the leakage area of the center chamber with the environment results in $A_{0,7} = 0$. Furthermore, it is obvious that only those cracks have to be taken into account, which have an intersection with the outer robot circle, because only those can cause a loss of negative pressure. This fact allows a rather efficient leakage simulation by pre-selecting the relevant cracks.

4.3 Simulated Seven-Chamber System

Figure 10 shows the simulated behavior if the robot drives across a crack (cross-section of crack: $80mm^2$ unsealed leakage area). At the beginning all valves (see bottom right figure) are opened a bit due to the basic leakage of $0.1mm$. At cycle time $t \approx 55steps$ the robot's first chamber (1) arrives at the crack and first arbitrary leakages occur. This results in a loss of negative pressure of about $250Pa$ (upper right figure) which is compensated by the control system. Valve 1 is opened to get more negative pressure from the reservoir chamber (lower right figure). Short time later the next two chambers (2,6) are above the crack and lose negative pressure. Because of the precondition that the negative pressure of the center chamber (7) must be lower than the one of the surrounding chambers, the corresponding valve must be opened more. The next leaky chambers are 3 and 5 followed by the last one (4). During this process the reservoir permanently loses negative pressure (increasing line in upper left figure) while it is supplying the other chambers, but the vacuum is still strong enough to compensate all occuring leakages so the robot will not fall down. After passing the crack the leakages diminish and the negative pressure of the reservoir chamber is restored to the desired value.

In cases of larger cracks it is necessary to cut off chambers with a high leakage by

closing the valve to the reservoir chamber. This causes a total loss of vacuum inside the specific chamber but prevents a system-wide propagation of normal pressure. The system is designed to absorb up to four deactivated chambers which is necessary for handling a large crack, if the remaining ones have low leakages.

5 Conclusion

We presented an outline of our climbing robot CROMSCI and discussed some components like the negative pressure system and thermodynamical model in detail. The comparison of simulated results and the one-chamber prototype indicates that the developed physical model is exact enough to estimate the efficiency of the proposed adhesion mechanism. The propulsion system has been tested extensively and allows high maneuverability on reasonably flat ground.

Future Work mainly consists of a completion of the adhesion system and experiments under real conditions. Some technical fine tuning will follow when we are able to validate the system's performance and the simulation model. A critical point in future will be the leak tightness and abrasion of the sealing facings. Here a few more experiments are necessary.

References

[Autumn et al., 2005] Autumn, K., Buehler, M., Cutkosky, M., Fearing, R., Full, R. J., Goldman, D., Groff, R., Provancher, W., Rizzi, A. A., Saranli, U., Saunders, A., and Koditschek, D. E. (2005). Robotics in scansorial environments. In *SPIE - The International Society for Optical Engineering*, volume 5804.

[Berns and Hillenbrand, 2001] Berns, K. and Hillenbrand, C. (2001). Robosense - a climbing robot to examine bridges and dams. In *32nd International Symposium on Robotics (ISR), Seoul/Korea*.

[Braun et al., 2007] Braun, T., Wettach, J., and Berns, K. (2007). A customizable, multi-host simulation and visualization framework for robot applications. In *13th International Conference on Advanced Robotics (ICAR07)*, Jeju, Korea.

[Brockmann, 2004] Brockmann, W. (2004). Towards low cost climbing robots. In *7th International Conference on Climbing and Walking Robots (CLAWAR)*, volume Workshop on Robots in Entertainment, Leisure and Hobby. Springer Verlag.

[Fischer et al., 2007] Fischer, W., Tache, F., and Siegwart, R. (2007). Magnetic wall climbing robot for thin surfaces with specific obstacles. In *6th International Conference on Field and Service Robotics (FSR)*.

[Hach, 2006] Hach, A. (2006). Entwicklung eines positionsbestimmungssystems für mobile roboter, optimiert für dsp strukturen. Projektarbeit, Technische Universität Kaiserslautern.

[Hägele, 2006] Hägele, M. (2006). Assistive robots in everyday's environments. Europe's Information Society - ICT Riga 2006.

[Hillenbrand and Berns, 2004] Hillenbrand, C. and Berns, K. (2004). A climbing robot based on under pressure adhesion for the inspection of concrete walls. In *35th International Symposium on Robotics (ISR)*, page 119, Paris, France.

[Hillenbrand and Berns, 2006a] Hillenbrand, C. and Berns, K. (2006a). The force controlled propulsion and adhesion system for a climbing robot. In *9th International Conference on Climbing and Walking Robots (CLAWAR)*.

[Hillenbrand and Berns, 2006b] Hillenbrand, C. and Berns, K. (2006b). Inspection of surfaces with a manipulator mounted on a climbing robot. In *37th International Symposium on Robotics (ISR)*.

[Hillenbrand et al., 2007] Hillenbrand, C., Schmidt, D., Berns, K., Leichner, T., Gastauer, T., and Sauer, B. (2007). Development of a sealing system for a climbing robot with negative pressure adhesion. In *10th International Conference on Climbing and Walking Robots (CLAWAR)*.

[Koch et al., 2005] Koch, J., Hillenbrand, C., and Berns, K. (2005). Inertial navigation for wheeled robots in outdoor terrain. In *5th IEEE Workshop on Robot Motion and Control (RoMoCo)*, Dymaczewo, Poland.

[Longo and Muscato, 2006] Longo, D. and Muscato, G. (2006). The alicia3 climbing robot. In *IEEE Robotics And Automation Magazine*.

[Luk et al., 2005] Luk, B. L., Cooke, D., Galt, S., Collie, A. A., and Chen, S. (2005). Intelligent legged climbing service robot for remote maintenance applications in hazardous environments. *Robotics and Autonomous Systems 53*, pages pp. 142–152.

[Menon et al., 2004] Menon, C., Murphy, M., and Sitti, M. (2004). Gecko inspired surface climbing robots. In *IEEE International Conference on Robotics and Biomimetics (ROBIO)*, Shenyang, China.

[Schmitz, 2005] Schmitz, N. (2005). Aufbau eines regelkreises zur druckregelung von vakuumkammern bei einem kletterroboter. Project Thesis, unpublished - Robotics Research Lab - University of Kaiserslautern.

[Scholl et al., 2001] Scholl, K. U., Albiez, J., and Gassmann, G. (2001). Mca- an expandable modular controller architecture. In *3rd Real-Time Linux Workshop*, Milano, Italy.

[Simons, 2006] Simons, F. (2006). *Verhalten von passiv betriebenen Sauggreifern unter der Krafteinwirkung von Kletterrobotern*. PhD thesis, Stuttgart, Univ., Fak. Maschinenbau, Inst. für Industrielle Fertigung und Fabrikbetrieb.

[Weise et al., 2001] Weise, F., Köhnen, J., Wiggenhauser, H., Hillenbrand, C., and Berns, K. (2001). Non-destructive sensors for inspection of concrete structures with a climbing robot. In *CLAWAR 2001, Karlsruhe, Germany, September 2001*.

[Wettach et al., 2005] Wettach, J., Hillenbrand, C., and Berns, K. (2005). Thermodynamical modelling and control of an adhesion system for a climbing robot. In *20th IEEE International Conference on Robotics and Automation (ICRA)*, Barcelona, Spain.

[Zhang et al., 2006] Zhang, H., Zhang, J., Zong, G., Wang, W., and Liu, R. (2006). Sky cleaner 3 - a real pneumatic climbing robot for glass-wall cleaning. In *IEEE Robotics And Automation Magazine*.

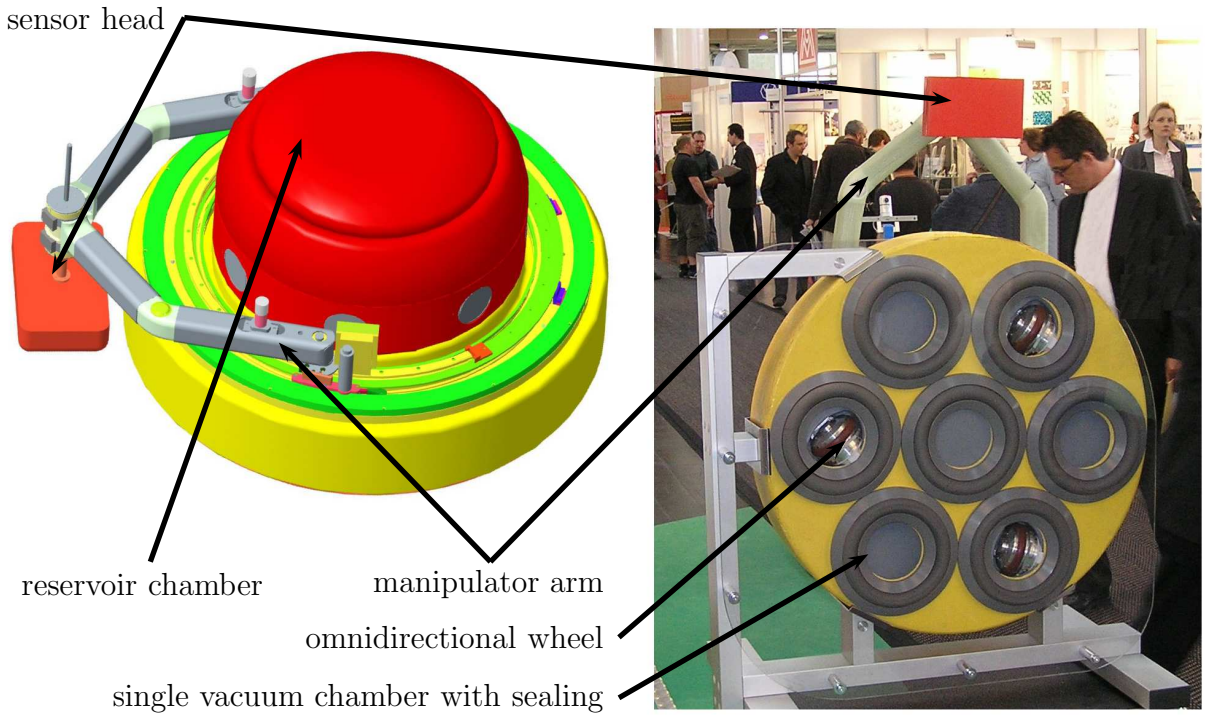

Figure 1: Construction drawing of CROMSCI (left, view on top) and as presented at the Hannover Messe 2007 (right, bottom view)

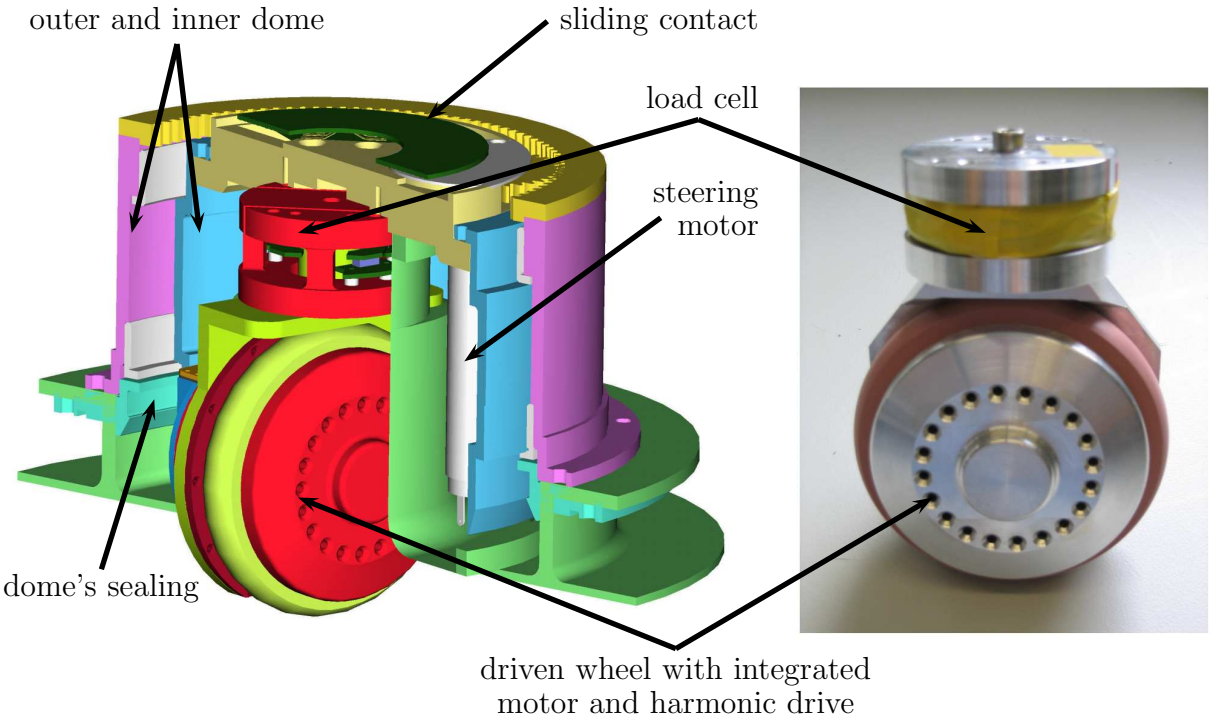

Figure 2: Construction drawing of a single wheel (left) and inner part (right)

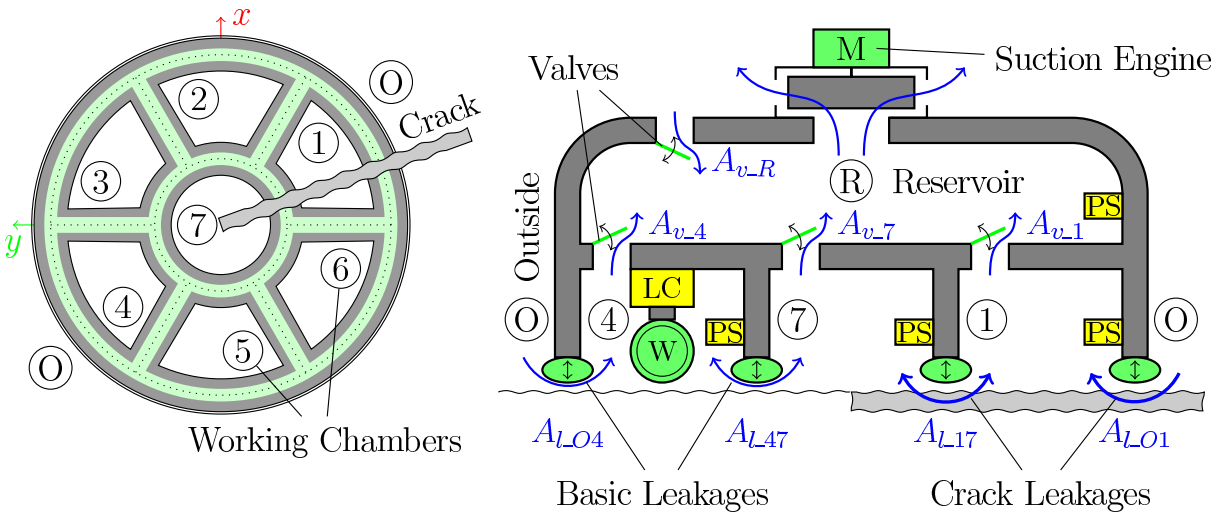

Figure 3: Division of suction chambers with an example crack (left) and overall elements and airflow (right)

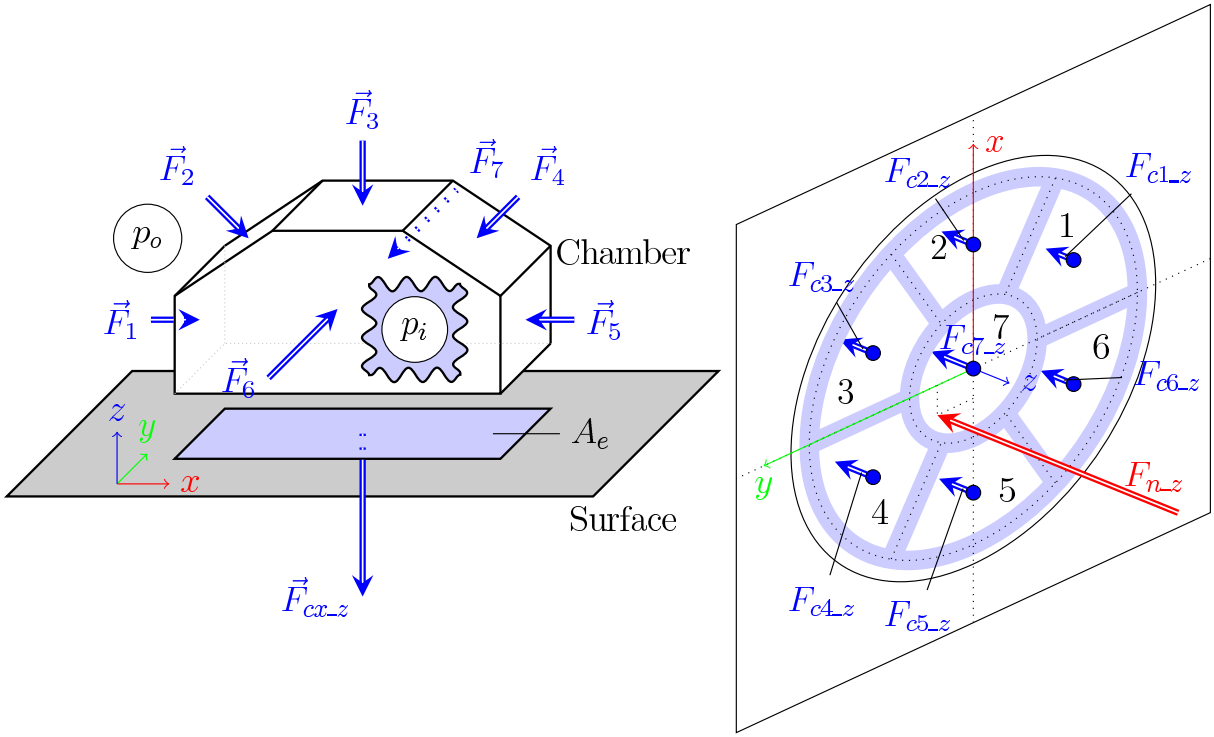

Figure 4: Forces which take effect on the robot

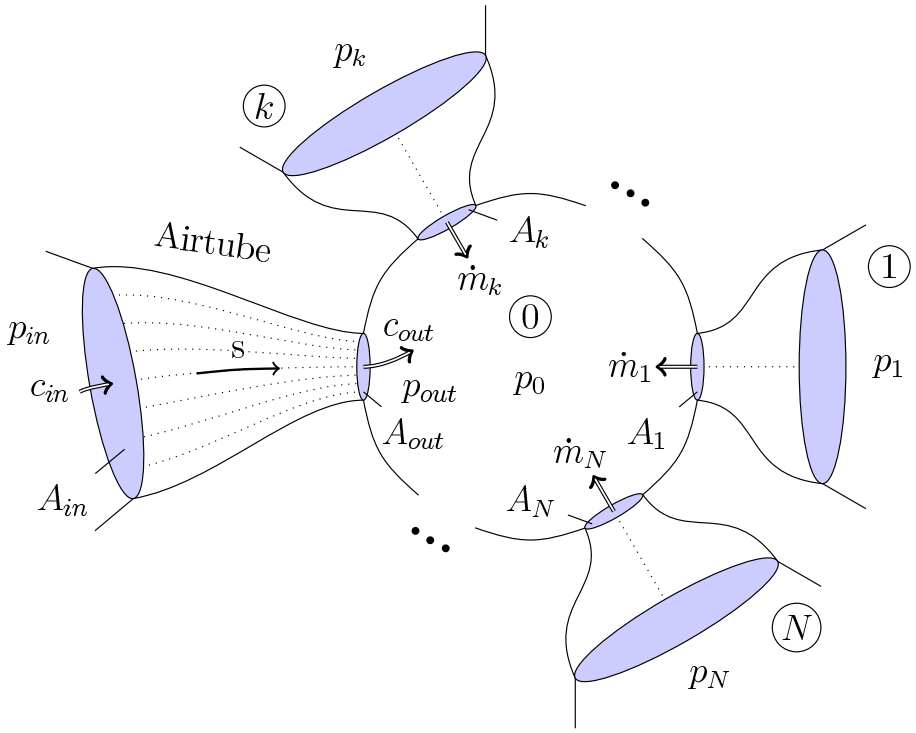

Figure 5: Modelling of airflow by an airtube

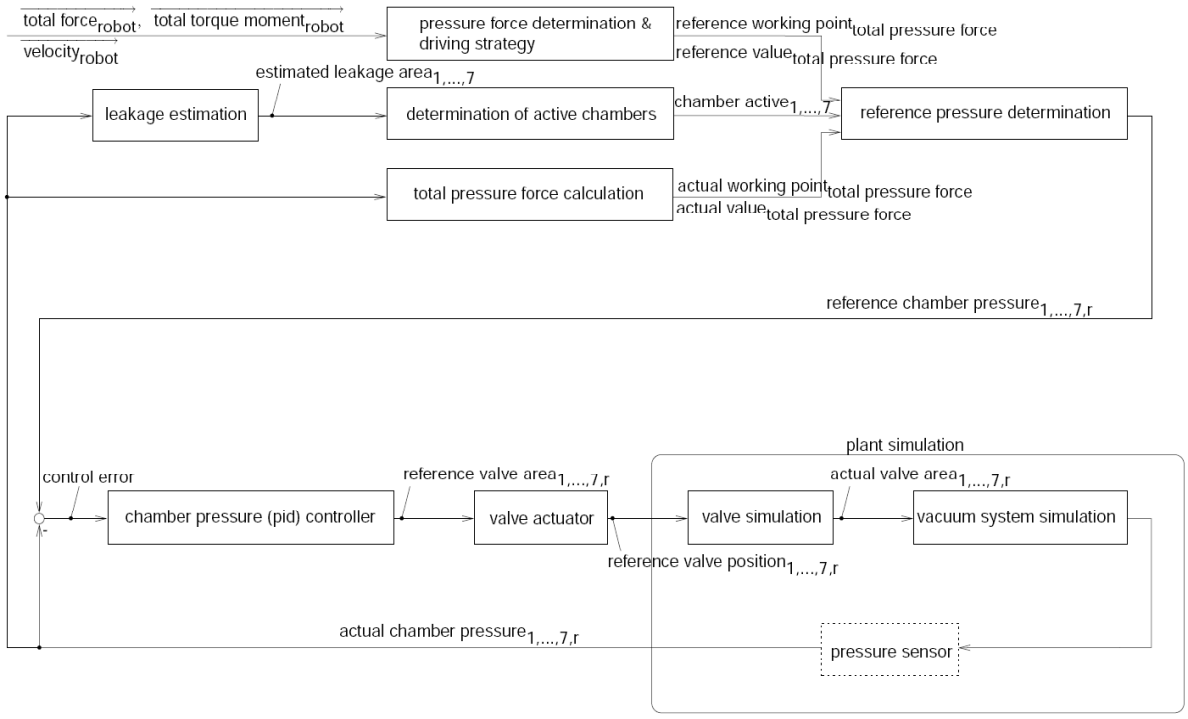

Figure 6: Structure of closed-loop pressure controller combined with simulation

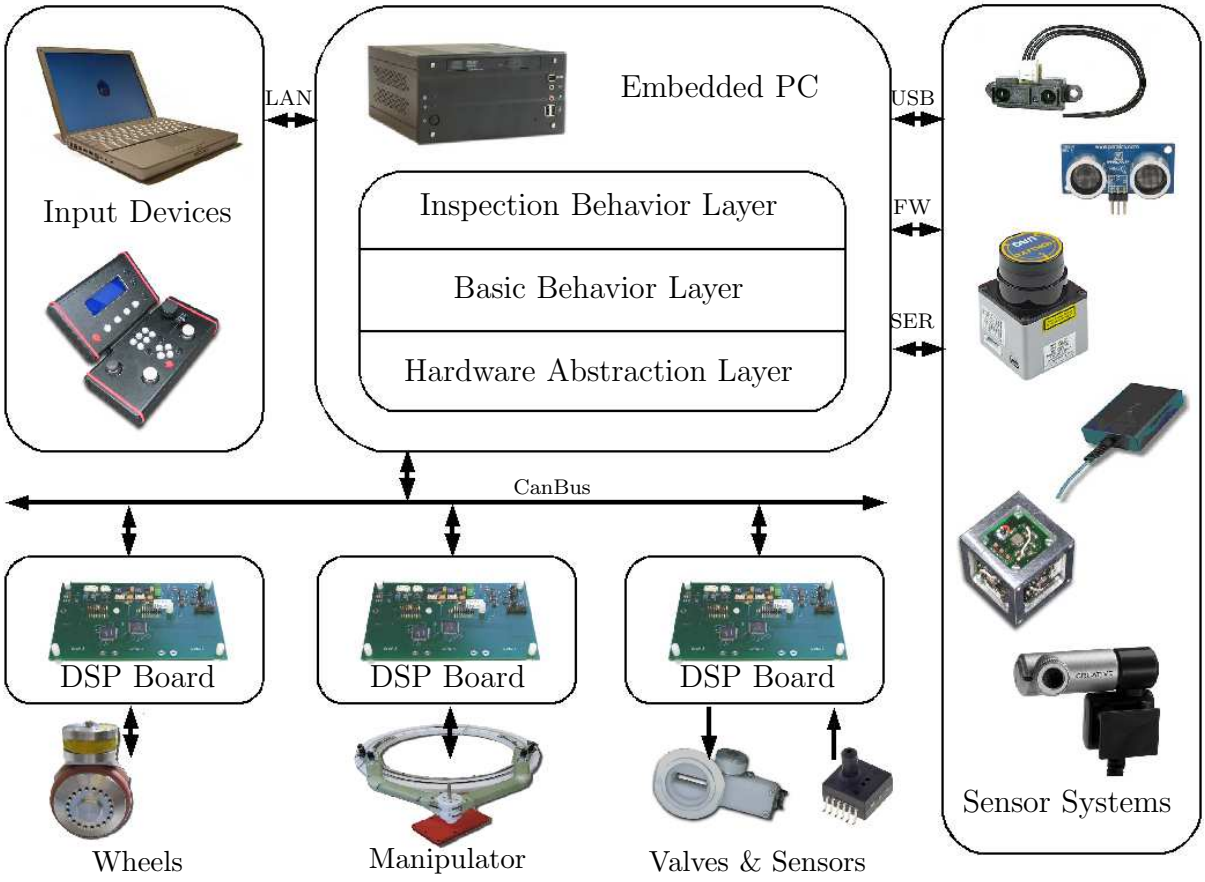

Figure 7: Overview of control architecture

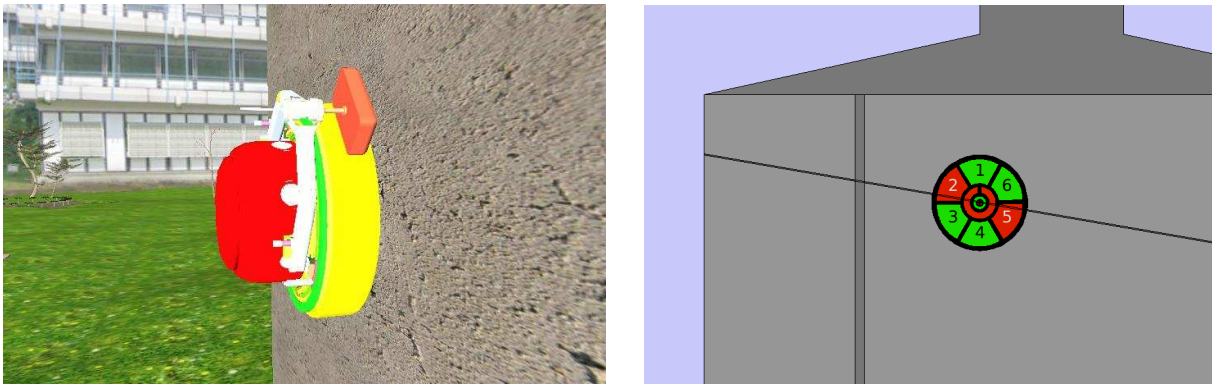

Figure 8: 3D-Visualization of robot at a bridge pylon (left) and crack simulation in 2D (right)

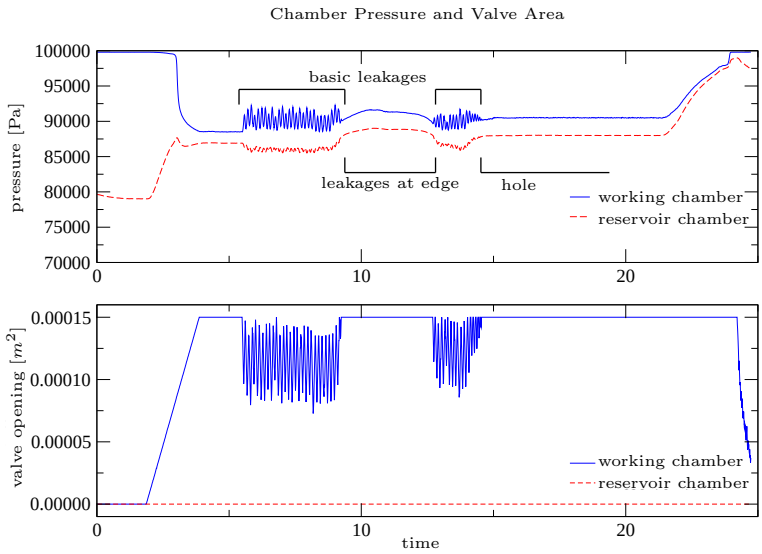

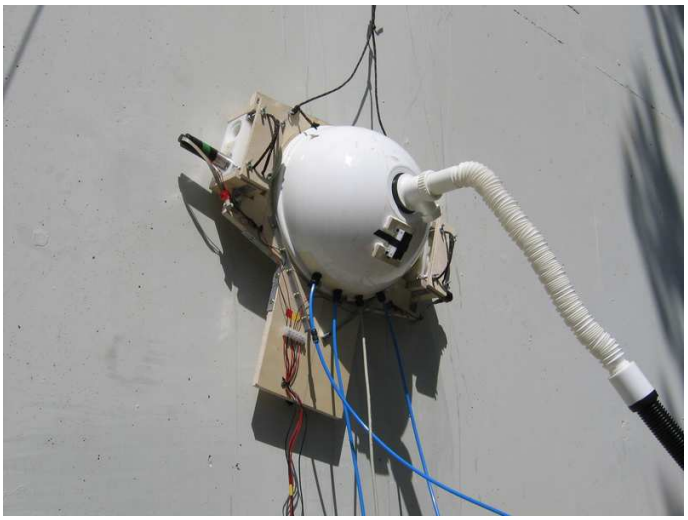

Figure 9: Results of an experiment with a leakage area of about $12mm^2$ at one-chamber prototype (bottom)

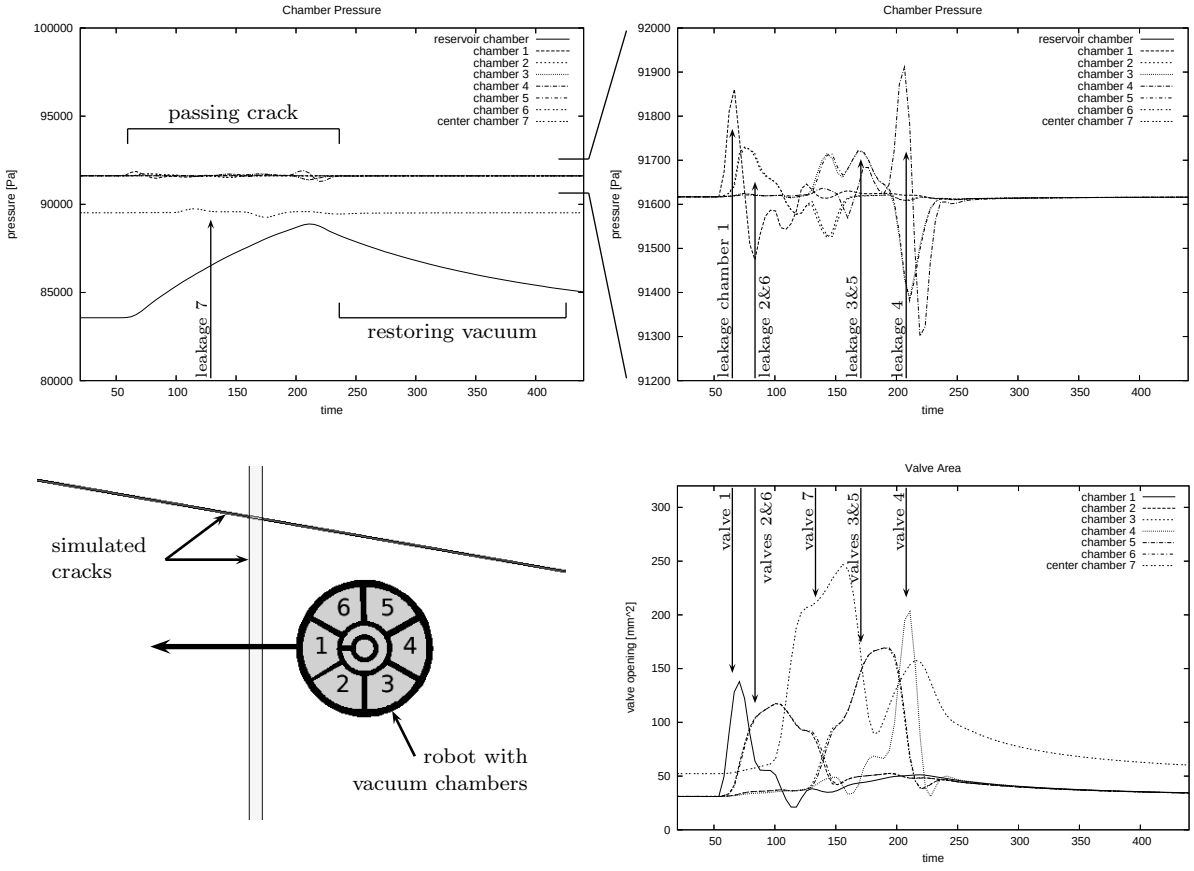

Figure 10: Simulated passing of a crack (bottom left) and resulting pressure values (top) and valve openings (bottom right)